Wettability of Electroplated Ni-P in Under Bump Metallurgy with Sn-Ag-Cu Solder

YUNG-CHI LIN,[1] JENQ-GONG DUH,[1,3] and BI-SHIOU CHIOU[2]

1.—Department of Materials Science and Engineering, National Tsing Hua University, Hsinchu, Taiwan. 2.—Department of Electronics Engineering, National Chiao-Tung University, Hsinchu, Taiwan. 3.—E-mail: jgd@mx.nthu.edu.tw

Nickel plating has been used as the under bump metallurgy (UBM) in the microelectronics industry. In this study, the electroplating process was demonstrated to be a good alternative approach to produce the Ni-P layer as UBM. The wettability of several commercial solder pastes, such as Sn-3.5Ag, Sn-37Pb, and Sn-3Ag-0.5Cu solder, on electroplated Ni-P with various phosphorous contents (7 wt.%, 10 wt.%, and 13 wt.%) was investigated. The role of phosphorus in the wettability was probed. The surface morphology and surface roughness in electroplated Ni-P was observed with the aid of both field emission scanning electron microscope (SEM) and atomic force microscope (AFM). The correlation between wettability and phosphorus contents in electroplated Ni-P was evaluated. As the phosphorous contents increased, the surface morphology of the Ni-P deposit was smoother and surface roughness of Ni-P became smaller. The improvement of surface morphology and surface roughness enhanced the wettability of electroplated Ni-P. The interfacial reaction between lead-free solder and electroplating Ni-P UBM was also investigated.

Key words: Lead-free solder, electroplated Ni-P, under bump metallurgy (UBM), wettability, interfacial reaction

INTRODUCTION

In the microelectronics industry, the flip-chip technology (FCT) with beneficial advantages has attracted focused attention for electronic packaging in consumer products.[1–3] Manufacturing of bumps on the die is the preliminary step for FCT. An under bump metallization, which is a multilayer structure, contains essential functions, such as adhesion to terminal electrode, the diffusion barrier between the solder and terminal electrode, and wettability for soldering. The nickel-based under bump metallurgy (UBM) has been widely used because of the rapid reaction of Sn with Cu and the spalling problem associated with Cu-Sn intermetallic compounds (IMCs).[4–10] Recently, the electroless nickel (EN) process is an alternative method to deposit Ni. However, the deposition rate of the EN process is rather slow and thus time-consuming. The electroplated Ni-P is suggested to be more effective in the fabrication of the Ni-P UBM. In the electroplating process,[11,12] the deposition rate is determined by the current density rather than the spontaneous chemical reaction, and could be as high as 50 μm/h. Besides, the relatively low working temperature around 50°C provides milder operation conditions and makes the process less energy intensive.

In this study, the surface morphology, surface roughness, and wettability between several commercial solder pastes and as-derived electroplated Ni-P were investigated. Furthermore, the interfacial reaction of SnAgCu lead-free solder on the electroplated Ni-P metallization layer was also probed and discussed.

EXPERIMENTAL PROCEDURE

The nickel-phosphorous layer was prepared by electrodeposition, and the Brenner-type bath[12] was used. The metallization layer employed was Ni-P deposit/Cu/Ti/Si. The top metal of Si wafer was Cu, which acted as an interconnection line. The adhesion layer was sputtered Ti of 1000 Å. A layer of 10-μm Ni-P was electroplated on the top of the electroplated Cu, which was then jointed with the solder

(Received February 28, 2005; accepted July 27, 2005)

paste. With various phosphoric acid (H_3PO_3) addition, Ni-P deposits with different P contents were obtained. The bath compositions in the deposition are presented in Table I. Table II shows the compositions of phosphorous contents in the Ni-P layer analyzed with an electron probe microanalyzer (EPMA, JXA-8800M, JEOL, Tokyo, Japan). After deposition, the electroplated Ni-P layer was immediately immersed in deionized water for 2 min and then dried with alcohol. As the UBM was plated onto the Si wafer, the commercial solder paste, Sn-3Ag-0.5Cu (SMIC, Senju Metal Industry Co., Tokyo, Japan), was then applied.

The Sn-3Ag-0.5Cu solder paste was placed on the Ni-P UBM and then reflowed three times. Solder reflows were carried out in a conducting solder reflow oven (Falcon 5 × 5 MultiPurpose System, SIKAMA, Santa Barbara, CA). The peak temperature of reflow profile for Sn-3Ag-0.5Cu pastes was set at 240°C.

An x-ray diffractometer (XRD-6000, Shimadzu, Kyoto, Japan) with a wavelength of $\lambda = 1.5406$ Å for Cu K_α was used to examine the crystallization of the electroplated Ni-P layer with different phosphorous contents.

The surface morphology of the electrodeposited Ni-P was observed with a field emission scanning electron microscope (FESEM, JSM-6500F, JEOL, Tokyo). The surface roughness of the Ni-P deposit was analyzed with the aid of an atomic force microscope (AFM, DI3100, Digital Instrument, New York, NY).

A dynamic contact angle analyzer system (FTA200, First Ten Angstroms) was used to measure the contact angle of several commercial solder pastes, such as Sn-3.5Ag, Sn-37Pb, and Sn-3.0Ag-0.5Cu solder, on electroplated Ni-P. The electroplated Ni-P/Cu/Ti/Si substrate with solder pastes was put into the heated environment chamber. During the melting process, live images were continuously captured by the grabber and transferred to the user screen. From the live images, the contact angle can be drawn and measured.

The interfacial morphologies of the solders and UBM were observed with an FESEM. The compositions of various phases in the solder joints and the corresponding elemental distribution across the joint interface were quantitatively measured with EPMA with the aid of a ZAF program.[13]

Table I. Compositions of Brenner-Type Bath for Electroplating Ni-P

Brenner-Type Bath at 50°C	Quantity (g/L)
$NiSO_4 \cdot 6H_2O$	150
$NiCl_2 \cdot 6H_2O$	45
$NiCO_3$	40
H_3PO_4	50
H_3PO_3	30, 20, and 15*
pH	1.8, 20, and 2.5**

*30 g/L, 20 g/L, and 15 g/L of H_3PO_3 were for high, medium, and low phosphorous contents of Ni-P, respectively.
**The pH value of the high, medium, and low phosphorous contents of Ni-P were 1.8, 2.0, and 2.5, respectively.

Table II. Compositions of EP Ni-P Deposited on Cu/Ti/Si Substrates

P Level	H_3PO_3 Contents (g/L)	Ni Contents (Wt.%)	P Contents (Wt.%)
High P	30	85.65 ± 0.56	13.58 ± 0.53
Medium P	20	88.62 ± 0.30	10.37 ± 0.24
Low P	15	91.71 ± 0.35	7.38 ± 0.36

RESULTS AND DISCUSSION

Composition of Electroplated Ni-P (EP Ni-P) Deposit

For the Brenner-type bath, the phosphorous content of the EP Ni-P deposit is affected by several operational parameters, such as amounts of phosphorous acid (H_3PO_3), current density, pH values of solution, and stirring rate. In this study, the effect of different phosphorous acid contents was investigated. The phosphorous contents of the EP Ni-P layer analyzed by EPMA are listed in Table II. The phosphorous content obtained at various H_3PO_3 additions of 15 g, 20 g, and 30 g per liter are about 7 wt.%, 10 wt.%, and 13 wt.%, respectively. It appears that the phosphorous content of EP Ni-P deposit increases with phosphorous acid. The deposition rate of EP Ni-P as a function of H_3PO_3 is represented in Table III. It is evident that the solution with less H_3PO_3 addition achieves a faster deposition rate of EP Ni-P.

Two types of mechanisms for electrochemical reaction of EP Ni-P deposit were reported: direct and indirect mechanisms.[14,15] The electrochemical reactions in both mechanisms shows that as the H^+ ions and $H_2PO_3^-$ ions decreased, the phosphorous contents of EP N-P deposit were reduced. In addition, as the H^+ ions increased, i.e., the pH value of solution decreased, and the current efficiency of EP Ni-P also decreased.[16] An explanation for this finding is that the greater the amount of H^+ ions that exist in the bath, the greater the amount of hydrogen evolution formed at the cathode. This demonstrates that the hydrogen ions act as a barrier at the cathode that

Table III. Deposition Rates of EP Ni-P with Different Phosphorous Contents

P Level*	H_3PO_3 (g/L)	Deposit Time (Min)	Thickness (μm)	Deposition Rate (μm/h)
High P	30	50	7.9 ± 1.2	9.6
	30	40	6.3 ± 0.9	
Medium P	20	30	13.6 ± 0.9	28.2
	20	20	8.9 ± 1.1	
Low P	15	17	9.6 ± 1.1	36
	15	15	8.4 ± 0.7	

*The compositions of low, medium, and high P were given in Table II.

disturbs the adsorption of nickel ions. In other words, the hydrogen ions increased since the nickel reduction was retarded. This indicates that increasing hydrogen ions results in the reduced deposition rate of EP Ni-P. In this study, as the H_3PO_3 addition increased, both H^+ and $H_2PO_3^-$ ions increased. Consequently, the higher phosphorous content of the EP Ni-P deposit and the lower deposition rate of the Ni-P layer were obtained when H_3PO_3 contents increased in the bath, as shown in Tables II and III.

Morphology and Structure of EP Ni-P with Various Phosphorous Contents

Figure 1 shows the surface morphology of the EP Ni-P deposited with various phosphorous contents. For the EP Ni-P with the high phosphorous content, the surface was rather flat and smooth. For the medium phosphorous Ni-P deposit, the surface became rougher than the high phosphorous ones, and the surface was composed by nodules. Relatively speaking, the low phosphorous one exhibited the roughest surface. The overall surface morphology was contributed to by small nodules in the low phosphorous deposit. It is revealed that the EP Ni-P deposited with fewer H_3PO_3 additions is accompanied by a rougher surface.

Figure 2 exhibits the surface morphology more clearly with the aid of AFM. These images were scanned from the area of 10 μm × 10 μm. The surface of the Ni-P layer with the high phosphorous content was relatively smooth. The medium phosphorous one was composed of small nodules ~1 μm in size. The Ni-P deposit with the low phosphorous content exhibited nodules and larger height difference. Nodules in the low phosphorous deposit were also around 1 μ, yet the deposit displayed larger height variation in the AFM image.

The surface roughness of the EP Ni-P deposit with various phosphorous contents is shown in Fig. 3. It is revealed that as the phosphorous contents increased, the surface roughness decreased. The surface roughness was about 6 nm for the high phosphorous content EP Ni-P. For the roughest one, i.e., the low phosphorous content EP Ni-P, the roughness of about 13 nm was still good enough to be an UBM. In our previous study,[17] the roughness of electroless deposited nickel (EN) UBM with various phosphorous contents was increased with decreasing phosphorous content. The surface roughness was 6–12 kÅ with phosphorous contents ranging from 6 wt.% to 13 wt.%. Such a rough surface for EN resulted from the rough substrate, i.e., 2~3 kÅ in Al_2O_3. Peeters and co-workers showed that the roughness between electroplated and electroless Ni-P was comparable.[18] In this study, the EP Ni-P could be deposited with a faster deposition rate than EN, and exhibited appropriate surface roughness. In fact, the surface roughness is one of the critical factors that can affect wettability between the solder paste and UBM.[19]

Table III reveals that the EP Ni-P bath with less H_3PO_3 adding exhibits a higher deposition rate. The

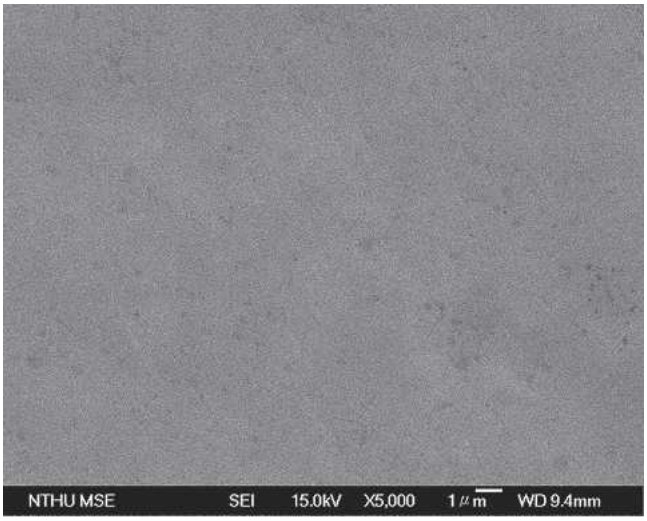

a

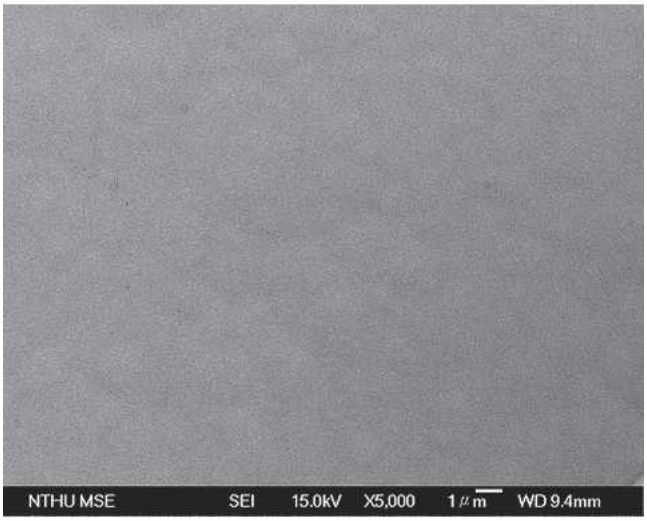

b

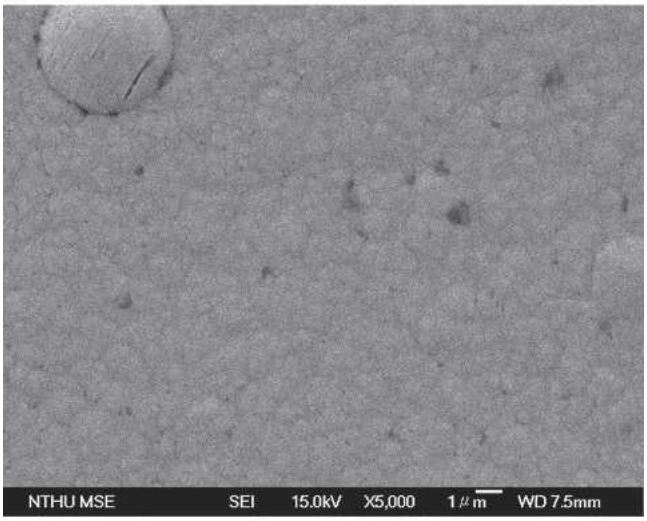

c

Fig. 1. Morphology of EP Ni-P deposited with various phosphorous contents.

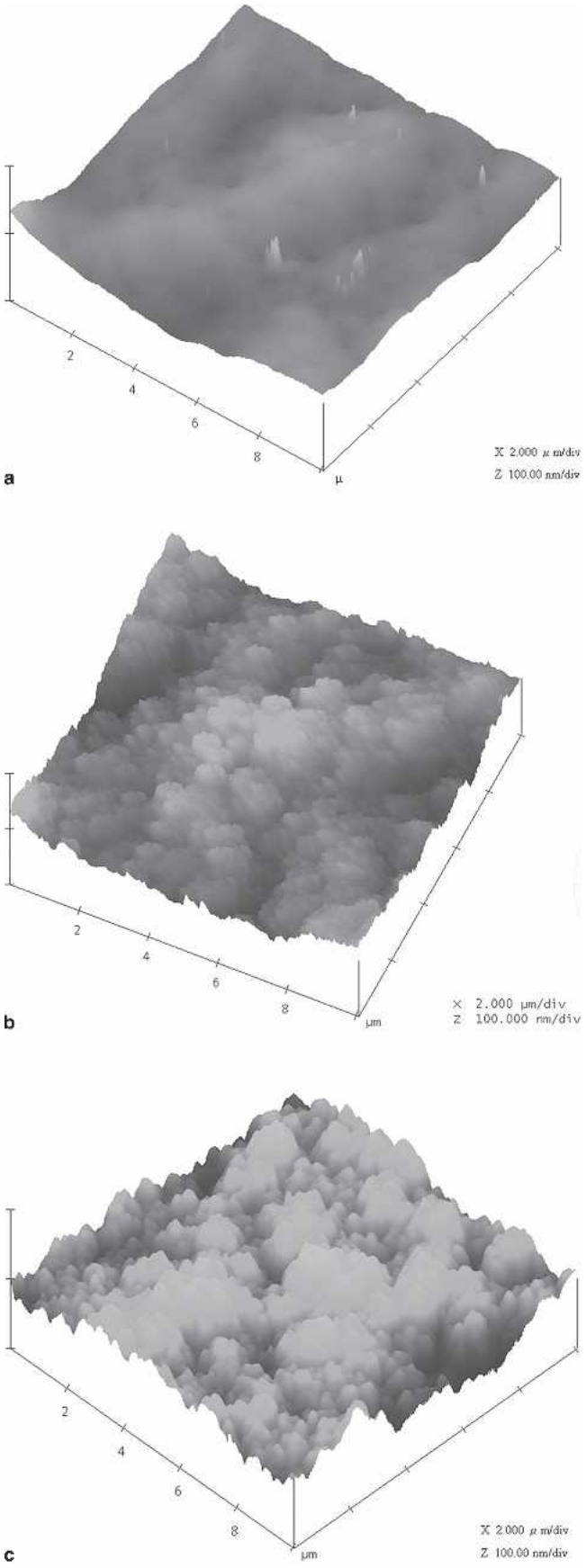

Fig. 2. AFM images of EP Ni-P deposited with different phosphorous contents.

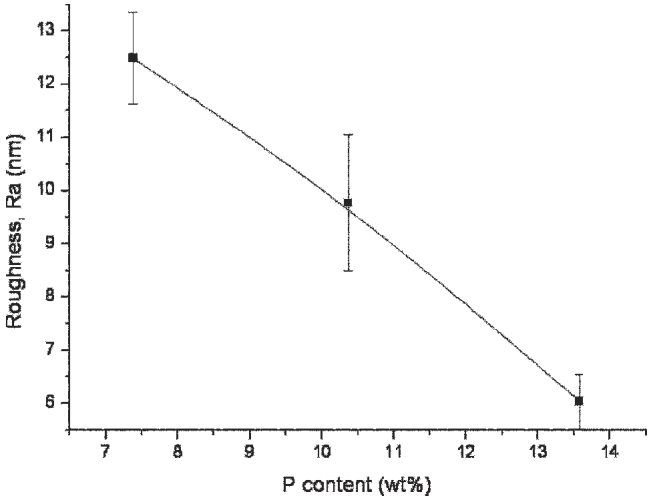

Fig. 3. Surface roughness of EP Ni-P deposited with difference phosphorous contents.

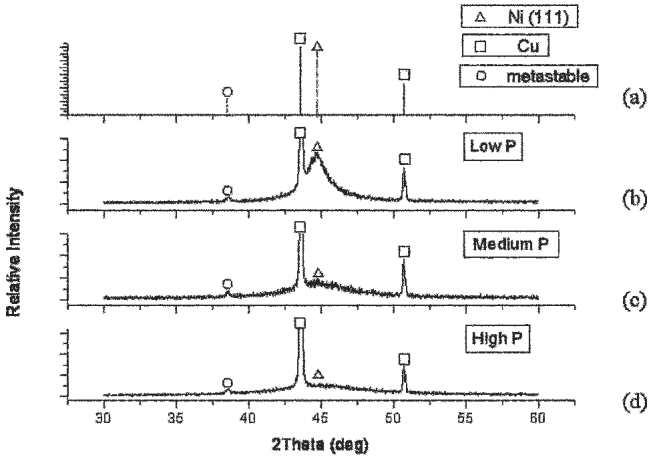

Fig. 4. XRD patterns of EP Ni-P with various phosphorous contents.

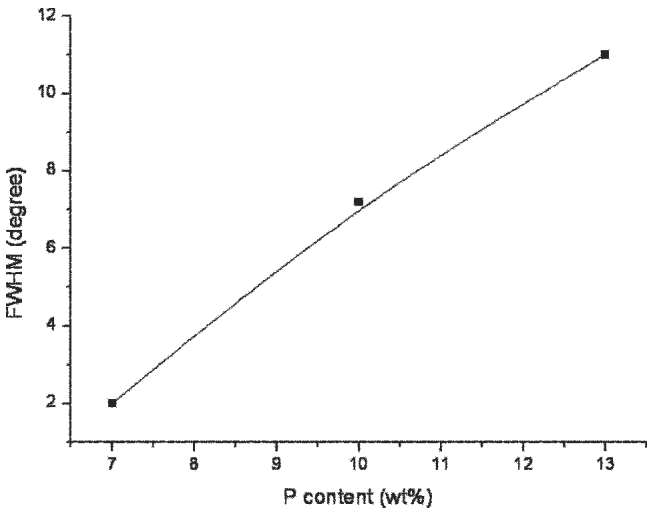

Fig. 5. FWHM of EP Ni-P on Cu/Ti/Si substrates with respect to phosphorous contents.

high depositing rate means a high nucleation rate of EP Ni-P, which may encapsulate more hydrogen during deposition. In fact, more hydrogen could be captured during deposit, and resulted in a lower

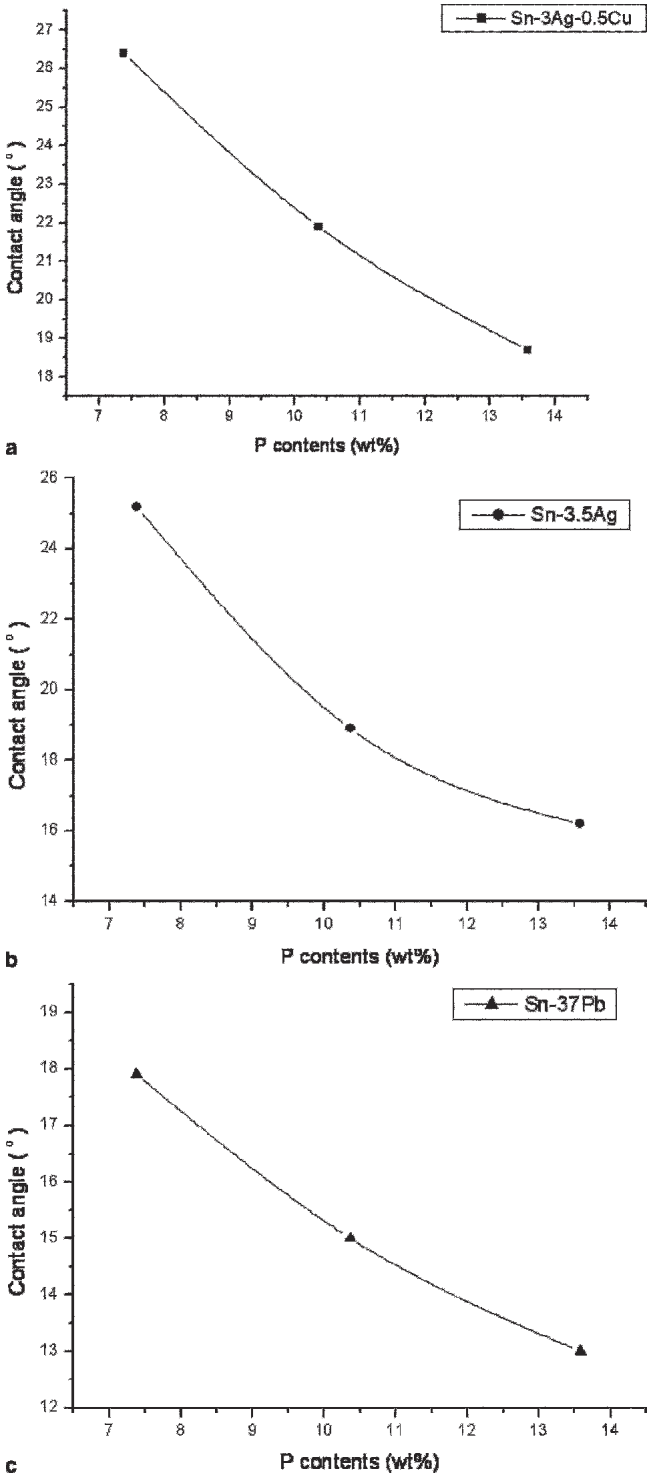

Fig. 6. The wetting angle of various commercial solder pastes on EP Ni-P as a function of P wt.%: (a) Sn-3Ag-0.5Cu, (b) Sn-3.5Ag, and (c) Sn-37Pb (eutectic SnPb).

density of atomic packing, leading to the higher surface roughness. Therefore, the EP Ni-P deposited with less H_3PO_3 addition achieves a lower phosphorous content of Ni-P layer, exhibiting higher surface roughness, as indicated in Fig. 3.

The XRD patterns for EP Ni-P deposited with various phosphorous contents are shown in Fig. 4. Two sharp peaks around 43° and 50° were from the

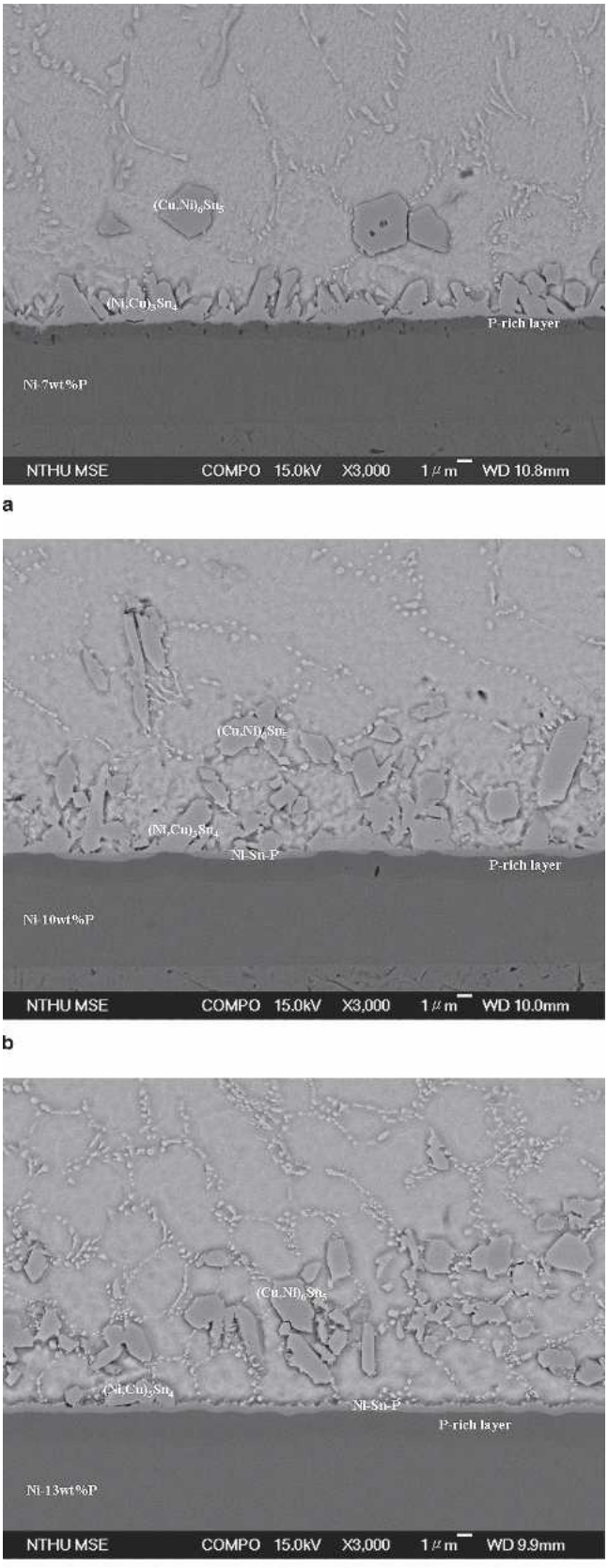

Fig. 7. Cross-sectional image of interfacial morphology in the Sn-3Ag-0.5Cu/EP Ni-P with various P content interfaces after three times reflows: (a) low P, (b) medium P, and (c) high P content EP Ni-P UBM.

Cu wetting layer, and the broadened peak around 44.5° was Ni (111). All the peaks positions are identified in Fig. 4a.

The phosphorous content of the Ni-P deposit significantly affected the crystallization of Ni. The EP Ni-P deposited with a low phosphorous content achieves a higher degree of crystallinity for a higher peak intensity of Ni (111), as shown in Fig. 4b. However, the EP Ni-P with a higher phosphorous content produces a lower degree of crystallinity, since the Ni (111) peak is much broader.

The degree of crystallinity for EP Ni-P can be further realized on the basis of the so-called full-width at half-maximum (FWHM). The large value of the FWHM peak represents the low degree of crystallinity. Figure 5 indicates that the value of FWHM calculated by the Lorentz method[20] increased with the phosphorous content of EP Ni-P. Therefore, the EP Ni-P deposited with either low or high phosphorous content was able to exhibit nanocrystalline and amorphous structure, respectively. It is believed that an elevated phosphorous content contained in EP Ni-P tends to disorder the lattice arrangement of Ni, and thus leads to a lower degree of crystallinity, as compared to that with lower phosphorous content.

Wettability between Commercial Solder Paste and EP Ni-P with Different Phosphorous Contents

The wetting angles of several commercial solder pastes, including Sn-3.5Ag, Sn-3Ag-0.5Cu, and eutectic Sn-37Pb, on EP Ni-P metallization, were studied at 240°C. Figure 6 gives the wetting angles of solder pastes on EP Ni-P with various phosphorous contents. For Sn-3Ag-0.5Cu solder paste on EP Ni-P with phosphorous content from 7 wt.% to 13 wt.%, the wetting angles were in the range between 18 and 27°, while the wetting angles of Sn-3.5Ag/EP Ni-P and Sn-37Pb/EP Ni-P ranged from 15° to 26° and 12° to 19°, respectively. The eutectic Sn-37Pb solder exhibited the smallest wetting angle, indicating the best wettability on EP Ni-P among these commercial solder pastes.

In fact, on the basis of wetting angle measurements, the wettability was comparable for Sn-3Ag-0.5Cu and Sn-3.5Ag. In the industry, the wetting angle is on the order of 35° between commercial solder paste and Cu UBM.[21] In this study, the wetting angle of these commercial solder pastes on EP Ni-P was smaller than 30°, which implied that the EP Ni-P layer was able to offer better wettability.

Among these commercial solder pastes, the eutectic SnPb solder showed the best wetting behavior. This may be attributed to the difference of melting point between eutectic SnPb and Sn-Ag based solder pastes. The melting points for eutectic SnPb, Sn-3.5Ag, and Sn-3Ag-0.5Cu are 183°C, 221°C, and 217°C, respectively. The larger the temperature difference between the test temperature (240°C) and melting point, the higher is the potential for atoms to diffuse. It is argued that eutectic SnPb with the largest temperature difference illustrates better wetting behavior with EP Ni-P than both Sn-3Ag-0.5Cu and Sn-3.5Ag.

Furthermore, the wetting behavior of solder pastes on the EP Ni-P was also dependent on the phosphorous content in Ni-P. The higher the phosphorous content, the lower the wetting angle, i.e., the better wettability. This can be related to the surface roughness of EP Ni-P with different phosphorous contents. As shown in Fig. 3, if the phosphorous content of Ni-P increased, the roughness of the EP deposit decreased, i.e., it became smoother. The decreasing roughness of the Ni-P surface made the solder spread more freely and easily during the reflow process and therefore the wetting angle was reduced, as shown in Fig. 6.

In the literature, Chen et al.[19] argued that surface roughness affected the wetting behavior between solder pastes and Cu UBM, and as the roughness of the Cu surface decreased, the wetting behavior was better. In the study of the wettability between lead-free solder and EN,[17] it was revealed that as the roughness of the EN surface increased, the wetting angle between the solders and EN decreased. The wettability of Sn-3.5Ag on EN was measured to be 60~90°. However, in this study, the wetting angle was as low as 16~26°. The surprising result can be related to the difference in substrate roughness. In the Young et al. study,[17] the substrate was commercial Al_2O_3 ceramic substrate with roughness about 2 kÅ, while the Cu/Ti/Si used as the substrate in this study was with a roughness of only several nanometers. Due to the substrate roughness distinction, the deposited Ni-P also exhibited the roughness variation between EN/Al_2O_3 and EP Ni-P/Cu/Ti/Si. The roughnesses of EN/Al_2O_3 and EP Ni-P/Cu/Ti/Si were 6 ~10 kÅ and 610 nm, respectively. It is apparent that the roughness of Ni-P significantly influences the wettability. A parallel study,[22] in which EN with about 9 wt.% phosphorous was deposited on

Table IV. Compositions of IMCs between Sn-3Ag-0.5Cu and EP Ni-P with Different Phosphorous Contents after Reflows

P Level	IMC Type	Sn (At.%)	Cu (At.%)	Ni (At.%)
High P	$(Ni, Cu)_3Sn_4$	57.7 ± 0.5	8.8 ± 0.9	33.3 ± 0.9
	$(Cu, Ni)_6Sn_5$	46.1 ± 0.4	30.3 ± 0.9	23.4 ± 0.9
Medium P	$(Ni, Cu)_3Sn_4$	57.2 ± 0.9	8.3 ± 0.6	34.4 ± 1.3
	$(Cu, Ni)_6Sn_5$	46.4 ± 0.6	31.1 ± 0.6	22.3 ± 0.8
Low P	$(Ni, Cu)_3Sn_4$	56.0 ± 0.4	8.2 ± 0.4	35.5 ± 0.6
	$(Cu, Ni)_6Sn_5$	45.6 ± 0.5	31.2 ± 1.0	22.9 ± 0.7

the Cu/Ti/Si substrate, showed the wetting angle between the Sn-3Ag-0.5Cu solder paste and the EN/Cu/Ti/Si to be around 20°. It appears that the wetting behavior between electroplated Ni-P and electroless Ni-P was comparable.

Interfacial Interaction between Sn-3Ag-0.5Cu Solder Paste and Electroplated Ni-P Layer after Reflow

In the electronic industry, the reflow process between the solder paste and UBM layer was critical. After the solder bump was electroplated onto the UBM layer, the electroplated solder was melted to form rotundity in an infrared reflow oven after the first reflow cycle. The chip would be assembled with the plastic substrate after the second reflow cycle. However, the assembly of some solder joints may not be as good as expected at this time, and a third time reflow cycle is thus required. In fact, the reflow cycles selected in this study reflect an actual process in the electronic industry.

The backscattered electron image (BEI) images of the Sn-3Ag-0.5Cu solder paste on the EP Ni-P with different phosphorous content after three times of reflow are shown in Fig. 7. It is revealed that after the reflow process, the IMCs formed and a P-rich layer also developed between the IMC and Ni-P layer. The shapes of IMCs were quite distinct as the phosphorous content varied. For the EP UBM with the low P content, there existed a continuous IMC attached on the Ni-P, and a few IMCs with darker color in the BEI image spalled into the solder after three times reflow.

With the aid of EPMA, the compositions of these IMCs were quantitatively analyzed. The composition of the continuous IMC was 56.0 ± 0.4 at.% Sn-35.5 ± 0.6 at.% Ni-8.2 ± 0.4 at.% Cu. The ratio of the atomic percentage of (Ni + Cu) to Sn was (35.5 + 8.2):(56), which is close to 3:4. Therefore, this IMC could be denoted as the $(Ni,Cu)_3Sn_4$ IMC. On the other hand, the spalled IMC was with 45.6 ± 0.5 at.% Sn-22.9 ± 0.7 at.% Ni-31.2 ± 1.0 at.% Cu, in which the atomic percentage ratio of (Ni + Cu) to Sn was (22.9 + 31.2):(45.6), and was close to 5:6. Thus, the $(Cu,Ni)_6Sn_5$ IMC was confirmed.

The compositions of IMCs for EP Ni-P UBM with low P, medium P, and high P content are listed in Table IV. For the Ni-P deposit with medium phosphorous content, significant amounts of IMCs were spalled into the solder. A thin Ni-Sn-P layer formed above the P-rich layer. The Ni-Sn-P layer grew intermittently adjacent to the P-rich layer. It is worthy to note that the IMC appeared to be attached well on UBM in the Ni-Sn-P free section, and almost no IMC was revealed adjacent to the Ni-Sn-P layer. For high phosphorous EP Ni-P, there was a continuous Ni-Sn-P layer on top of the P-rich layer. Nearly all the IMCs were spalled into the solder paste. It is argued that the spalled IMCs were associated with the Ni-Sn-P layer. As the phosphorous content in EP Ni-P increased, the Ni-Sn-P layer grew thicker and became more continuous. Figure 8 showed the Ni-

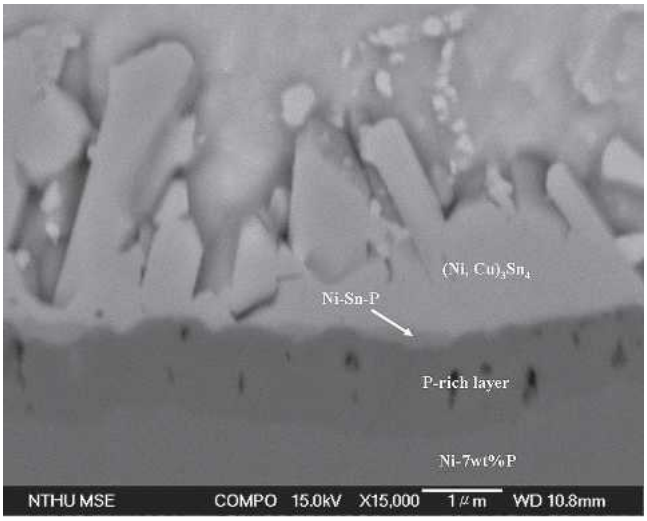

a

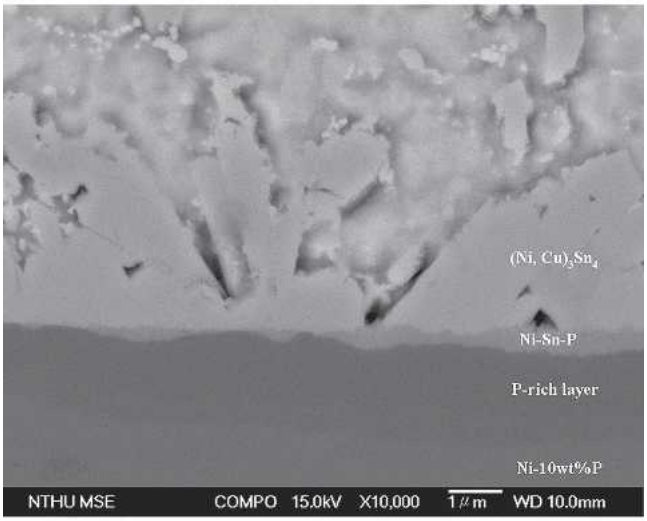

b

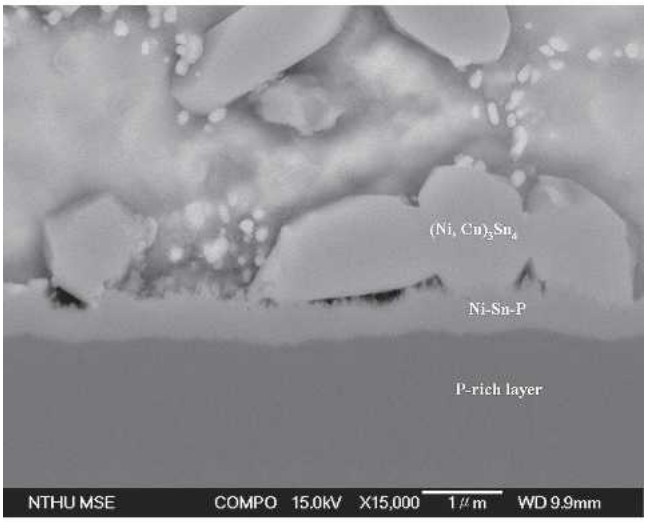

c

Fig. 8. The SEM images of Ni-Sn-P layer between $(Ni, Cu)_3Sn_4$ and P-rich layer: (a) low P, (b) medium P, and (c) high P content EP Ni-P UBM.

Sn-P layer between (Ni, $Cu)_3Sn_4$ and the P-rich layer on the Ni-P UBM. In fact, the growth of the Ni-Sn-P layer was also found in the case of the EN UBM. Sohn et al. demonstrated the increase of the IMC spalling with P content in the EN UBM.[23] Kim et al. reported that the Ni-Sn-P layer grew as reflow time increased.[24] It appears that the interfacial reaction between the solder pastes and EP Ni-P UBM was similar to the reactions between the solder paste and EN UBM.

In this study, the surface roughness of the EP Ni-P and its wettability, as well as the interfacial reaction between solder pastes and the EP Ni-P, were intensively investigated. It is apparent that the results in the EP Ni-P were comparable to those of the EN. Nevertheless, the EP Ni-P was much more time effective than the EN, because of the relatively slow deposition rate of EN. In addition, an 8 h long passivation time for the deposited sample was also required for EN. Therefore, the electroplating process was demonstrated to be a good alternative approach for producing the Ni-P layer as UBM.

CONCLUSIONS

The contact angles of eutectic SnPb solder paste on the EP Ni-P with 7–13wt.%P ranged from 12° to 19°. For Sn-3.5Ag/EP Ni-P and Sn-3Ag-0.5Cu/EP Ni-P joints, the contact angles were 15–26° and 18–27°, respectively. The wetting behavior was degraded with decreasing phosphorous contents in Ni-P for all three solder pastes. The IMC formation of the interfacial reactions in solder/EP Ni-P joints after reflows was quite different for various contents of EP Ni-P. The formation of the Ni-Sn-P layer may be the critical factor. The higher the phosphorous content in the EP Ni-P layer, the thicker and more continuous was the observed growth of the Ni-Sn-P layer.

The electroplated Ni-P deposit was fabricated with a faster deposition rate, almost triple that of the EN. The surface roughness, wettability, and interfacial reaction between the EP Ni-P/solders were comparable to those for the EN. Although the electroplated process consumed electricity, the EP process exhibited a much faster deposition rate, and no passivation was required. Therefore, the electroplating process was demonstrated to be a better approach to producing the Ni-P layer as UBM.

ACKNOWLEDGEMENT

The financial support from the National Science Council, Taiwan, under Contract No. NSC-93-2216-E-007-014 is acknowledged.

REFERENCES

1. J.H. Lau, *Flip Chip Technologies* (New York: McGraw-Hill, 1996), pp. 26–30.
2. D.S. Patterson, P. Eleniu, and J.A. Leal, *Adv. Electron. Packaging* 1, 337 (1997).
3. C.S. Chang, A. Oscilowski, and R.C. Bracken, *IEEE Circuits Dev. Mag.* 14, 45 (1998).
4. A.A. Liu, H.K. Kim, K.N. Tu, and P.A. Totta, *J. Appl. Phys.* 80, 2774 (1996).
5. H.K. Kim, K.N. Tu, and P.A. Totta, *Appl. Phys. Lett.* 68, 2204 (1996).
6. K.L. Lin and Y.C. Liu, *49th Electronic Components and Technology Conf. (ECTC)* (Piscataway, NJ: IEEE, 1999), pp. 607–612.
7. B.L. Young and J.G. Duh, *J. Electron. Mater.* 30, 878 (2001).
8. C.S. Huang, J.H. Yeh, B.L. Young, and J.G. Duh, *J. Electron. Mater.* 31, 1230 (2002).
9. S.K. Kang, R.S. Rai, and S. Purrshothaman, *J. Electron. Mater.* 25, 1113 (1996).
10. J.W. Nah and K.W. Paik, *IEEE Trans. Compon. Packaging Technol.* 25, 32 (2002).
11. A. Brenner, G.E. Riddell, and J. Res, *Nat. Bur. Standards* 39, 35 (1947).
12. A. Brenner, *Electrodeposition of Alloys: Principles and Practice* (New York: Academic Press, 1963), pp. 457–483.
13. J.I. Goldstein, *Scanning Electron Microscopy and X-ray Microanalysis* (New York: Plenum Press, 1992), pp. 306–330.
14. R.L. Zeller III and U. Landau, *J. Electrochem. Soc.* 138, 1010 (1991); R.L. Zeller III and U. Landau, *J. Electrochem. Soc.* 139, 464 (1992).
15. T.M. Harris and Q.D. Dang, *J. Electrochem. Soc.* 140, 81 (1993).
16. T. Morikawa, T. Nakade, M. Yokoi, Y. Fukumoto, and C. Iwakura, *Electrochim. Acta* 42, 115 (1997).
17. B.L. Young, J.G. Duh, and B.S. Chiou, *J. Electron. Mater.* 30, 543 (2001).
18. P. Peeters, G.V.D. Hoorn, T. Daenen, A. Kurowski, and G. Staikov. *Electrochim. Acta* 47, 161 (2001).
19. Y.Y. Chen, J.G. Duh, and B.S. Chiou, *J. Mater. Sci.: Mater. Electron.* 11, 279 (2000).
20. B.D. Cullity and S.R. Stock, *Elements of X-Ray Diffraction,* 3rd ed. (Englewood Cliffs, NJ: Prentice-Hall, 2001), pp. 145–150.
21. *http://www.yikst.com/Page/YIKSTE.html*
22. S.T. Kao, Y.C. Lin, and J.G. Duh, *J. Electron. Mater.* (in press).
23. Y.C. Sohn and J. Yu, *J. Mater. Res.* 19, 2428 (2004).
24. S.W. Kim, J.W. Yoon, and S.B. Jeng, *J. Electron. Mater.* 33, 1182 (2004).